

Near Infrared Light Sensitive Ultraviolet–Blue Nanophotoswitch for Imaging-Guided “Off–On” Therapy

Jing Zuo,^{†,‡,||} Langping Tu,^{†,||} Qiqing Li,[†] Yansong Feng,[‡] Ivo Que,[§] Youlin Zhang,[†] Xiaomin Liu,[†] Bin Xue,[†] Luis J. Cruz,[§] Yulei Chang,^{*,†} Hong Zhang,^{*,‡} and Xianggui Kong^{*,†}

[†]State Key Laboratory of Luminescence and Applications, Changchun Institute of Optics, FineMechanics and Physics, Chinese Academy of Sciences, Changchun, 130033 Jilin, China

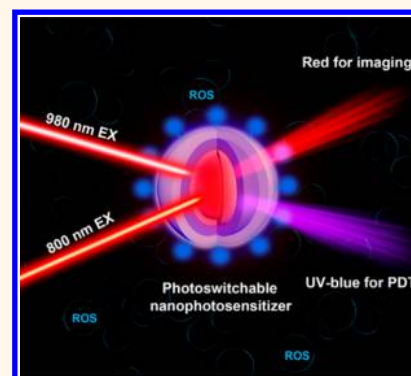
[‡]Van't Hoff Institute for Molecular Sciences, University of Amsterdam, Science Park 904, 1098XH Amsterdam, The Netherlands

[§]Translational Nanobiomaterials and Imaging, Department of Radiology, Leiden University Medical Center, 2333ZA Leiden, The Netherlands

Supporting Information

ABSTRACT: Photoswitchable materials are important in broad applications. Recently appeared inorganic photoswitchable upconversion nanoparticles (PUCNPs) become a competitive candidate to surmount the widespread issue of the organic counterparts—photobleaching. However, current PUCNPs follow solely Yb³⁺/Nd³⁺ cosensitizing mode, which results in complex multilayer doping patterns and imperfectness of switching in UV–blue region. In this work, we have adopted a new strategy to construct Nd³⁺ free PUCNPs—NaErF₄@NaYF₄@NaYbF₄:0.5%Tm@NaYF₄. These PUCNPs demonstrate the superior property of photoswitching. A prominent UV–blue emission from Tm³⁺ is turned on upon 980 nm excitation, which can be completely turned off by 800 nm light. The quasi-monochromatic red upconversion emission upon 800 nm excitation—a distinct feature of undoping NaErF₄ upconversion system—endows the PUCNPs with promising image-guided photoinduced “off–on” therapy in biomedicine. As a proof-of-concept we have demonstrated the imaging-guided photodynamic therapy (PDT) of cancer, where 800 nm excitation turns off the UV–blue emission and leaves the emission at 660 nm for imaging. Once the tumor site is targeted, excitation switching to 980 nm results in UV–blue emission and the red emission. The former is used to induce PDT, whereas the latter is to monitor the therapeutic process. Our study implies that this upconversion photoswitching material is suitable for real-time imaging and image-guided therapy under temporal and spatial control.

KEYWORDS: photoswitch, upconversion, photodynamic therapy, imaging, nanoparticle



Photoswitchable emission materials have been attracting global research interest in the aspects of both fundamental and technological advances, which stems from the emerging applications in ultrahigh-density optical data storage, optoelectronic devices, chemical sensing and especially biomedicine.^{1–4} Until now, most of the photoswitchable materials were based on organic fluorescent molecules and their derivatives, whose photostability is always a concern due to the inherent photobleaching.^{5–7} As an alternative, multilayer doping nanostructures based on lanthanide-doped upconversion nanoparticles (UCNPs) possessing narrowband excitation and multiband emission of lanthanide ions are proposed to be highly photostable and photoswitchable.^{8–12} Typically, UCNPs have the capability to convert near-infrared excitation light to ultraviolet (UV)-visible emission upon sequential multiphoton absorption or energy transfer, which is very attractive in

biomedicine since it may lead to deep tissue penetration, minimal autofluorescence background, and low photodamage of tissue.^{13–15} Benefit from the developed ~800 nm excitable Nd³⁺/Yb³⁺ cosensitized UC system^{16–18} and ~980 nm excitable Yb³⁺-sensitized UC system, in these years, the lanthanide-doped photoswitches have been successfully applied in inducing chemical reactions and others, such as switching of organic compounds,^{10,19} reversible regulation of cell–molecules interaction,²⁰ reversible handedness inversion¹² and orthogonal excitations–emissions coregulated therapy.^{11,21}

Received: October 18, 2017

Accepted: February 28, 2018

Published: February 28, 2018

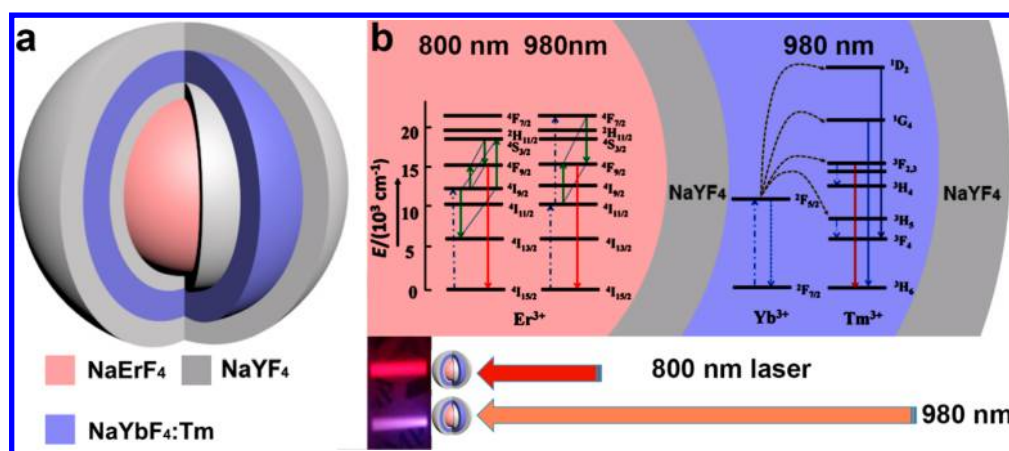


Figure 1. (a) The core–multishell structure of PUCNP. (b) Illustration of the composition of the PUCNP and its energy level diagrams under 980 and 800 nm NIR excitations, respectively. The designed structure results in wavelength-dependent emissions in the luminescent NaErF₄ core and NaYbF₄:Tm shell under dual NIR excitations.

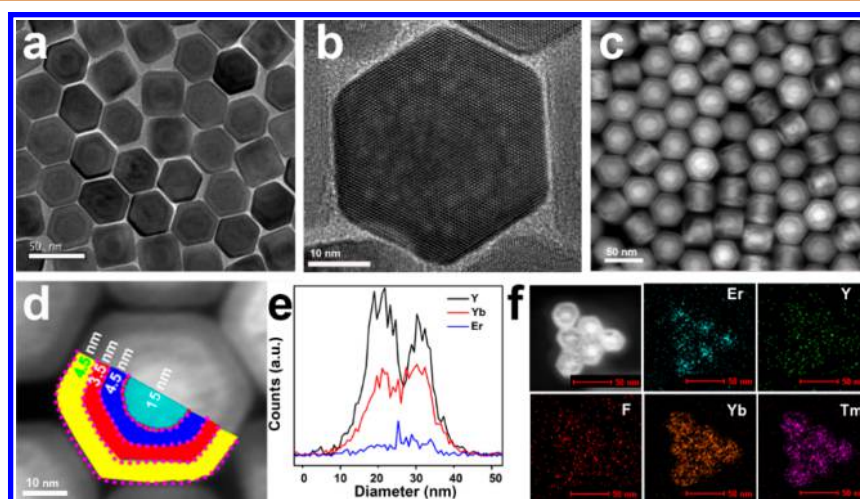


Figure 2. (a) TEM image of PUCNPs. (b) High-resolution TEM image of single PUCNP. (c) HAADF-STEM image of PUCNPs. (d) The magnified HAADF-STEM image of PUCNP for shell thickness measurement. (e) The HAADF-STEM-EDS mapping image of randomly selected PUCNP. (f) The electron energy loss spectroscopy (EELS) analysis results of six PUCNPs, the scale bars in (f) are 50 nm.

However, limited by the doping elements of suitable spectroscopic properties, all the reported upconversion photoswitches until now are restricted to Nd³⁺ and Yb³⁺ cosensitizing materials,²² which are complex in structure since it requests different doping patterns in different layers (see Figure 3b), and accompanied by a leakage in switch function—certain emission region cannot be completely closed (Figure S2).¹⁰

These restrictions can be lifted with recent advances in doping approaches of UCNPs. Last year, Almutairi *et al.*,²³ Liu *et al.*,²⁴ and our team²⁵ have independently reported that an effective upconversion luminescence can be realized in undoping NaErF₄@NaYF₄ (or NaLuF₄, NaGdF₄ shell *etc.*) nanostructures. Compared with conventional sensitizer/activator codoping systems, this type of upconversion material system possesses very interesting UC luminescence properties, *e.g.*, prominent quasi-monochromatic red upconversion emission of Er³⁺ and much weaker emission in UV–visible region,^{23–25} owing to the ladder-like energy levels of Er³⁺, the robust Er³⁺–Er³⁺ cross relaxation and the suppression of concentration quenching effect by shell protection, which shed light on developing high quality and less complex photoswitchable upconversion nanostructures.

In this work, we have successfully realized a complete photoswitching in UV–blue region with the structure: NaErF₄@NaYF₄@NaYbF₄:0.5%Tm@NaYF₄, in which the monochromatic red emission occurs upon ~800 nm excitation, whereas strong UV and blue emissions, besides the red emission, appear upon ~980 nm excitation (Figure 1 and 3a). Compared with the reported photoswitching UCNPs, our design is (1) Nd³⁺-free, which has only one doping layer avoiding complex doping pattern in multiple layers and simplifies the synthesis, and (2) a complete photoswitching of Er³⁺ in UV–blue region (*e.g.*, ~380 nm, ~410 nm) due to the robust Er³⁺–Er³⁺ cross relaxation in the undoped NaErF₄ core, which ensures the UV–blue emission coming solely from the UC emission of Tm³⁺. Given by this, the PUCNPs offer an alternative strategy for imaging-guided “off–on” phototherapy. More importantly, the nanoplatforms based on the PUCNPs could in principle circumvent the harmful effect of photo-damage caused by the “always ON” UV–blue light during diagnosis, which highlights the bioapplications of lanthanide-based UC nanomaterials.

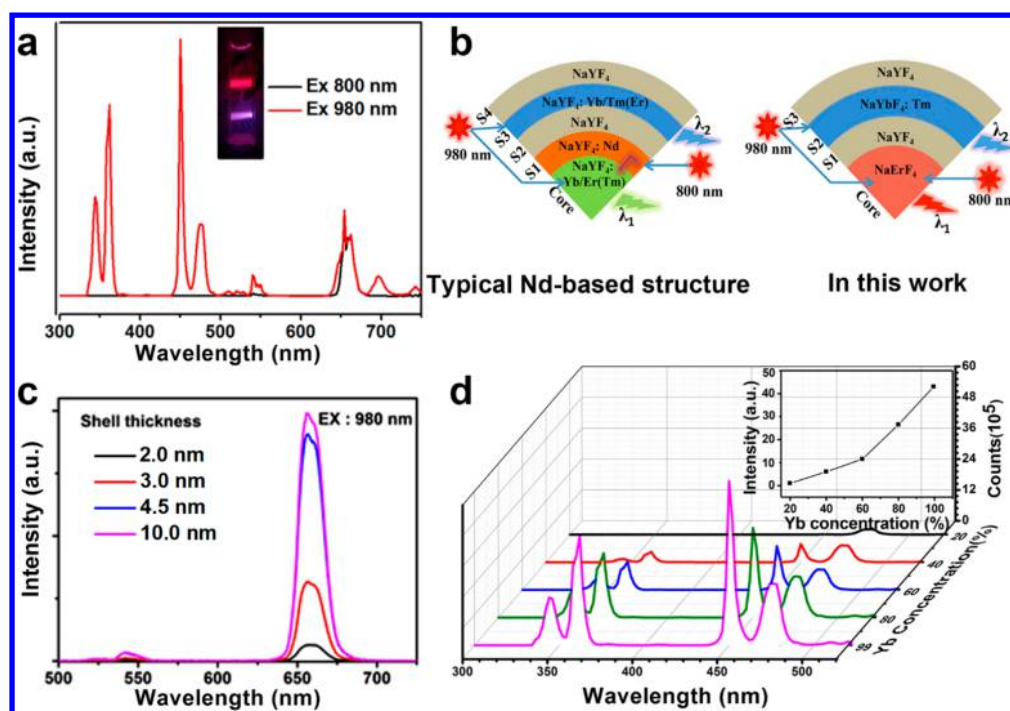


Figure 3. (a) Upconversion emission spectra of $\text{NaErF}_4@NaYF_4@NaYbF_4:0.5\%Tm@NaYF_4$ PUCNPs under 800 or 980 nm excitations at 5 W/cm^2 . The insert photograph shows the PUCNPs in cyclohexane solution under irradiation by two laser beams of 0.8 W/cm^2 . (b) Structure and photoswitch principles of NaErF_4 -based PUCNPs in this work and the conventional Nd-based ones. (c) UC luminescence spectra of different shell thicknesses of $\text{NaErF}_4@NaYF_4$. (d) UC luminescence spectra of the $\text{NaYF}_4@NaYF_4:x\%Yb,0.5\%Tm@NaYF_4$ (x : 20–99.5) core-shell-shell nanoparticles as a function of Yb^{3+} content in the middle layer. Excitation is CW 980 nm laser of 5 W/cm^2 . Inset: the Yb^{3+} concentration dependent UC emission intensity (integrated from 250 to 500 nm) of each type of core-shell-shell nanoparticles.

RESULTS AND DISCUSSION

The general core-multishell nanostructure of PUCNPs is a prerequisite to ensure the realization of such photoswitching function. The as-designed $\text{NaErF}_4@NaYF_4@NaYbF_4:0.5\%Tm@NaYF_4$ (C–S1–S2–S3, C = core, S = shell) nanostructure was synthesized by successive deposition of epitaxial multi shells. Figure 2a and b present the transmission electron microscopy (TEM) images of the PUCNPs, ensuring the uniform size and morphology of the nanoparticles with an average diameter of $\sim 40 \text{ nm}$. Furthermore, the high-angle annular dark field scanning transmission electron microscopy (HAADF-STEM) images shown in Figure 2c confirm the core-multishell structure of PUCNPs as the heavier lanthanide elements (Er and Yb, brighter parts) and the lighter ones (Y, darker parts) of the nanoparticle are distinguishable here. The sizes (or thickness) of the core and each shell are around 15 nm, 4.5 nm, 3.5 nm, 4.5 nm, respectively (as shown in Figure 2d). HAADF-STEM-EDS mapping (Figure 2e) and electron energy loss spectroscopy (EELS, Figure 2f) reaffirm the lanthanide ions distributions in such PUCNPs, in agreement with the result of Figure 2c. The hexagonal phase of the obtained PUCNPs is confirmed by X-ray diffraction (XRD) pattern (Supporting Information, Figure S1).

The corresponding photoswitching properties of the PUCNPs are displayed in Figure 3a. Upon excitation at 800 nm, only the monochromatic red emission ($\sim 660 \text{ nm}$) appears in the UV-visible region originated from the $\text{NaErF}_4@NaYF_4$ core-S1 part. Interestingly, upon 980 nm excitation, the UC red emission from the core-S1 part remained and the UV and blue emissions resulting from the S2–S3 part ($\text{NaYbF}_4:0.5\%Tm@NaYF_4$) appear—a typical photoswitching process. As shown in Figure 3b, compared with the previously reported photoswitch

structures, the PUCNPs not only simplify the structure by avoiding the Nd^{3+} -doped layer and complex doping patterns in different layers, but also offer a better spectral regulation in the UV-blue region. All these advantages are attributed to the introduction of the Er^{3+} -based self-sensitized UC system (NaErF_4), which makes it possible to build an efficient 800 nm triggered UCNP-based photoswitch without Nd^{3+} -sensitized layer. If we go over the conventional UC switches based on $\text{Yb}^{3+}\text{-Er}^{3+}$ or $\text{Nd}^{3+}/\text{Yb}^{3+}\text{-Er}^{3+}$ combination, the non-negligible UV-blue UC emission of Er^{3+} (e.g., ~ 410 and $\sim 380 \text{ nm}$, see Figure S2 in SI) is always a negative factor (*vide supra*). This defect can be overcome in our structure where the UV-blue emissions (even the green emission) of Er^{3+} are sufficiently quenched due to the robust $\text{Er}^{3+}\text{-Er}^{3+}$ cross-relaxation in the NaErF_4 core. As shown in Figure S2, compared with the traditional $\text{Nd}^{3+}/\text{Yb}^{3+}$ sensitized UC structure, the NaErF_4 -based structure reduces the UV-blue emission by at least 1 order of magnitude, while the red emission remains effective. Therefore, our design guarantees a better control of UV-blue emission, which is in favor of photoswitching involved applications (e.g., real-time UCL imaging and imaging-guided treatment).

Next, we optimize the structure of the PUCNPs. As far as the luminescence is concerned, the structure can be divided into two parts, namely, the $\text{NaErF}_4@NaYF_4$ core-S1 part and $\text{NaYbF}_4:0.5\%Tm@NaYF_4$ S2–S3 part. For the first part, the S1 shell thickness is important. As shown in Figure 3c, the UC luminescence of this part is significantly increased when the NaYF_4 shell gets thicker, until $\sim 4.5 \text{ nm}$, which is in line with our previous report.²⁵ Besides, thicker S1 layer blocks better the energy transfer between the luminescent core (NaErF_4) and S2 layer ($\text{NaYbF}_4:0.5\%Tm$), in favor of strong UC luminescence.

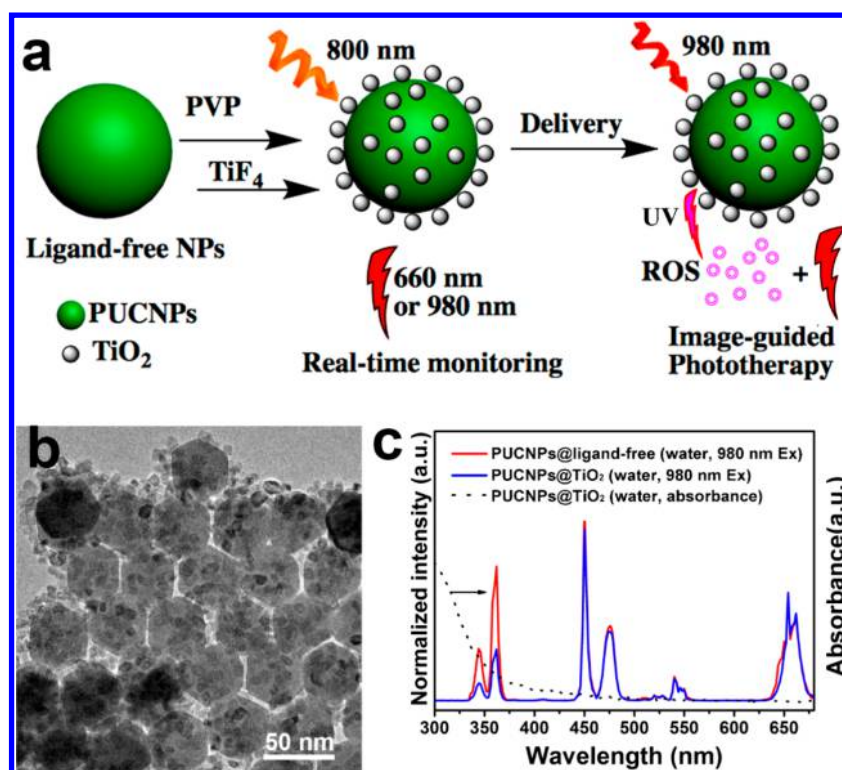


Figure 4. (a) Scheme of photoswitchable PDT using PUCNPs@TiO₂ for real-time monitoring and image-guided phototherapy. (b) TEM image of PUCNP@TiO₂ nanoparticles. (c) Upconversion emission spectra of PUCNPs@ligand-free (red line) and PUCNPs@TiO₂ (blue line), the corresponding absorbance of PUCNPs@TiO₂ is given as the dotted line.

As shown in Figure S3, if S1 layer is not thick enough, say less than ~ 4.5 nm in our case, the components of the two parts will be diffused to a certain extent to the S1 layer which is unavoidable during the high temperature synthesis, and the diffused ions may interact with each other in the S1 layer which shall significantly reduce the UC emission of S2 layer (the UC emission of Tm³⁺ can be well quenched by the diffused Er³⁺). This argument is further supported by the quenching effect of Nd³⁺ since Nd³⁺ is known to play the role of energy trap for the UC emission of Er³⁺. Thus, we have designed NaErF₄@NaYF₄@NaYF₄:80%Nd sandwich nanostructure (see Figure S4 for details). It is found out that only when the barrier layer is thicker than ~ 4.5 nm, the quenching effect of Nd³⁺ on the NaErF₄ core could be completely ignored, in agreement with results of Figure S3. Therefore, in the structure studied, the S1 layer thickness is set as ~ 4.5 nm.

As to the second part, high doping concentration of Yb³⁺ is used to achieve a robust UV–blue emission, which is rationalized by a simple sandwich structure: NaYF₄@NaYF₄:x%Yb0.5%Tm@NaYF₄ (x : 20–99.5). With the similar sizes (38 ± 3 nm) and morphologies of as-synthesized UCNPs (confirmed by the SEM images in Figure S5), the UC emission is enhanced significantly with the increase of Yb³⁺ concentration, as shown in Figure 3d. Compared to the most popular doping concentration (*i.e.*, 20%), Yb³⁺ concentration of 99.5% results in 40 times enhancement (emission intensity integrated range from 250 to 500 nm). This effect is ascribed to “size confinement effect” in the specific inert core–active shell–inner shell nanostructure.²⁶ On the basis of the above results and discussion, the PUCNP is optimized as NaErF₄(~ 15 nm)@NaYF₄(~ 4.5 nm)@NaYbF₄:0.5%Tm(~ 3.5 nm)@NaYF₄(~ 4.5 nm).

These PUCNPs are feasible for the application in theranostics. We demonstrate here, as a proof-of-concept, the features of separately controlling the upconversion luminescence (UCL) imaging (diagnosis) and photodynamic therapy (PDT) of cancer using PUCNPs@TiO₂ nanophotosensitizers (NanoPS). Considering that the photocatalyst-titanium dioxide (TiO₂) can only absorb UV light to catalyze the generation of reactive oxygen species (ROS), the PUCNPs@TiO₂ NanoPS can induce PDT only by 980 nm excitation (as shown in Figure 4c). The synthesis and photoswitching function of NanoPS are illustrated in Figure 4a. 800 nm laser excitation only generates quasi-monochromatic red emission for UCL imaging as diagnosis. Once the tumor site is targeted, the excitation shall switch to 980 nm to induce additional UV emission for PDT. Therefore, the photoswitching manner of the designed NanoPS guarantees the safety of imaging and the precision of therapy. The TEM image in Figure 4b reveals that some TiO₂ nanoparticles are decorated on the surface of PUCNPs as antennas, indicating the successful preparation of the PUCNPs@TiO₂ nanoplatform. Furthermore, the selective energy transfer efficiency between PUCNPs and TiO₂ is identified to 63%, as calculated from the dropped UV/red emission ratio subject to the TiO₂ modification (Figure 4c).

Before the application of PUCNPs@TiO₂ *in vivo*, its dark cytotoxicity was evaluated *in vitro* using A549 cells (Human lung adenocarcinoma epithelial). As shown in Figure S6, cell viability is higher than 85% even with a relatively high concentration (800 $\mu\text{g}/\text{mL}$) of PUCNPs@TiO₂. To study the cell imaging profiles, A549 cells were incubated with the PUCNPs@TiO₂ at 200 $\mu\text{g}/\text{mL}$ overnight and the cell nuclei were stained by DAPI, giving the blue emission as shown in Figure 5a. According to the overlapped channels, the UCL of PUCNPs@TiO₂ appears around the nucleus, indicating the

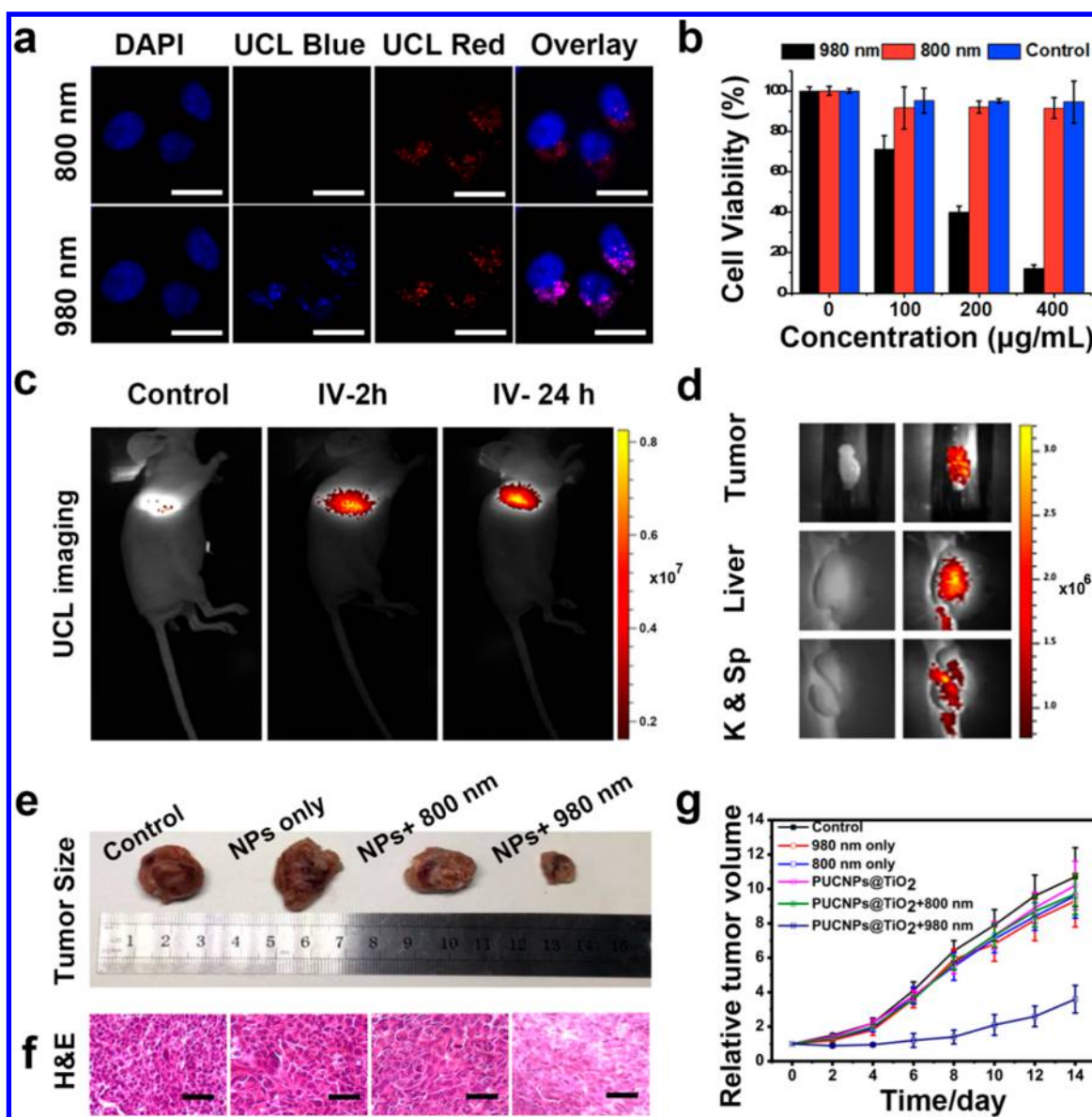


Figure 5. (a) A549 cells treated with PUCNPs@TiO₂ for imaging with 980 and 800 nm light excitation, respectively, and stained with DAPI. The scale bars are 20 μm . (b) A549 cells treated with PUCNPs@TiO₂ upon 800 and 980 nm laser irradiation with the same power densities. (c) *In vivo* UCL imaging of LLC tumor-bearing mouse with PUCNPs@TiO₂ under 800 nm laser at 2 and 24 h after intravenous injection. (d) *Ex vivo* UCL images of kidney, spleen, liver and tumor after 24 h post injection, the luminescent intensity of dissected organs further confirmed the preferential accumulation of PUCNPs@TiO₂ in tumor and main organs. (e) Photographs to display the excised tumors after various treatment. (f) H&E staining tumor sections harvested from the control group, groups of PUCNPs@TiO₂ only and PUCNPs@TiO₂ + 800 nm and PUCNPs@TiO₂ + 980 nm laser. The scale bars are 50 μm . (g) Relative tumor volumes change during the treatment ($n = 5$).

cellular internalization of the nanoplateform. Comparison between the UCL blue and red channels under different laser excitations (980 and 800 nm, respectively) comes out that only 980 nm excitation induces a bright blue UCL, whereas the red UCL can be generated by both 980 and 800 nm excitation.

Subsequently, the ROS generation of PUCNPs@TiO₂ nanoplateform was studied, where fluoresceinyl cypridina luciferin analogue (FCLA) was used as a specific chemiluminescence probe of ¹O₂ and O₂⁻. As shown in Figure S7, 980 nm excitation of the nanoplateform results in a cumulative chemiluminescence—a symbol of the increase of ROS generation. On the contrary, 800 nm light irradiation has no such effect. The corresponding standard curves are given as well to reconfirm it. Importantly, the intracellular ROS generation was also confirmed by the nonfluorescent DCFDA probe,

which could be deacetylated and further oxidized by ROS to the fluorescent DCF.²⁷ In Figure S8, compared to the control group and 800 nm laser treated group, the 980 nm laser treated group is proved to have effective generation of ROS, showing the strong fluorescence. The results above confirm the mechanism of ROS-mediated photoswitchable PDT.

Following the confirmation of ROS generation, the PDT effect of PUCNPs@TiO₂ against A549 cancer cells was evaluated by MTT assay. Dark toxicity, as a control, was also evaluated. After 24 h cell incubation, the difference in cell viability is clear when switching the wavelengths of irradiation. Upon 980 nm laser irradiation at 1 W/cm², the cell viability (as shown in Figure 5b) decreases significantly, which is more profound with higher drug dosage. For example, at 400 $\mu\text{g/mL}$ concentration, cell viability is down to 15%, indicating a robust

therapeutic effect. But there is no treatment effect under 800 nm laser excitation with the same light dosage.

On the basis of the *in vitro* results, the *in vivo* UCL imaging and photoswitchable PDT were then carried out. For UCL imaging, intravenous (IV) injection was conducted on tumor-bearing mice with 100 μL of PBS or PBS containing PUCNPs@TiO₂ (10 mg/mL). At 2 and 24 h after the injection, the tumor-bearing mice were exposed to the nontherapeutic 800 nm laser, as shown in Figure 5c. Compared to the control group, after 2 h the group of mice injected with the as-designed nanoplateform has already exhibited strong UCL in the tumor sites. Twenty-four hours later, the UCL intensity is observed to increase in the same area. Our results suggest the ability of PUCNPs@TiO₂ to accumulate in tumor site with the time increasing owing to the enhanced permeability and retention (EPR) effect. Then all the tumors and major organs of these mice were taken out for the *ex vivo* UCL imaging (Figure 5d). The tumor of the mice treated with PUCNPs@TiO₂ shows a strong luminescence signal. The signals are also observed in liver, spleen and kidney, while negligible signals are observable in other organs such as heart, lung (not provided). The results can qualitatively reflect the distribution of PUCNPs@TiO₂ in the body after IV injection.

For photoswitchable PDT, Lewis lung carcinoma (LLC) tumor-bearing C57BL/6 mice were intravenously injected with PUCNPs@TiO₂, and the tumor part was irradiated by 980 and 800 nm laser with the same light dosage at 0.5 W/cm² for 15 min irradiation (3 min irradiation each time with 3 min interval), respectively. In addition, the group injected with UCNPs@TiO₂ without laser irradiation, the group only irradiated by 980 or 800 nm laser, as well as the group without any processing, were set as control groups. As shown in Figure 5e, the excised tumors from these groups have confirmed the inhibition effect—the tumor size under 980 nm triggered PDT treatment is the smallest, whereas there is no significant difference among the other groups, even for the 800 nm triggered PDT treatment group with the same light dosage, which features the advantage of the as-designed photoswitchable PUCNPs@TiO₂ NanoPS in separating diagnosis (800 nm laser excitation) and photodynamic therapy (980 nm laser excitation).

To further confirm the therapeutic effect, the histological changes of corresponding excised tumors were evaluated by using hematoxylin and eosin (H&E) staining in Figure 5f. There are more significant damages in tumor cells with the injection of PUCNPs-TiO₂ (with 980 nm irradiation) than those in control groups. The histological analysis was also performed in heart, liver, spleen, lung and kidney (as shown in Figure S9) and no pathological changes were observed between the untreated group and 980 nm triggered PDT treatment group, indicating the harmlessness of the PUCNPs-TiO₂ NanoPS to normal organs. According to the overall therapeutic effect as shown in Figure 5g, only the group received the injection of PUCNPs@TiO₂ and 980 nm irradiation exhibits a significant PDT effect as evidenced by the lowest tumor growth rate. By contrast, the tumors of the other control groups grow continuously under the same conditions. Thus, the as-designed PUCNPs can be a candidate for NIR light-triggered photoswitchable nanoplateform with potential application in precise medicine.

CONCLUSION

In conclusion, a Nd³⁺ free photoswitchable upconversion nanomaterial, *i.e.*, NaErF₄@NaYF₄@NaYbF₄:0.5%Tm@NaYF₄ is realized. This structure succeeds in a complete photoswitching in UV–blue region, compared to the current Nd³⁺ photoswitching materials. The features of this nanostructure are (1) the core is dopant free, and thus a prominent quasi-monochromatic red upconversion emission of Er³⁺ is realized, (2) the intermediate layer thickness is set to 4.5 nm to avoid diffusion effect, and (3) the doping concentration of Yb³⁺ ions is raised to 99.5% to simplify the sandwich structure and achieve the robust UV–blue upconversion emission. As a proof of concept, we have constructed PUCNPs@TiO₂ as photoswitchable nanophotosensitizers to demonstrate its ability of imaging-guided “off–on” therapy. Our results indicate that this photoswitchable upconversion nanostructure can be expected to have promising applications in biomedicine.

MATERIALS AND METHODS

Reagents. RECl₃·6H₂O (Re: Y, Yb, Er, Nd, Tm > 99%), oleic acid (OA, 90%), 1-octadecene (ODE, 90%), oleylamine (70%), CF₃COONa, (CF₃COO)₃Y and TiF₄ were purchased from Sigma-Aldrich. RE₂O₃ (Re: Tm, Yb) was purchased from Aladdin. NaOH, NH₄F, methanol, ethanol and cyclohexane were purchased from GFS Chemical. Fluoresceinyl cypridina luciferin analogue (FCLA) was obtained from Tokyo Kasei Kogyo Co., Tokyo, Japan. All the chemicals were of analytical grade and there was no further purification. The cell lines used in this study were obtained from Basic Medical Sciences, Jilin University.

Preparation of PUCNPs. In order to synthesize the multishelled NaErF₄@NaYF₄@NaYbF₄:0.5%Tm@NaYF₄ nanoparticle, an epitaxial layer-by-layer growth Ostwald ripening method was employed.²⁸ The precursors of each shell were prepared in advance. The synthesis of bare core (NaErF₄) was following a previously reported procedure with some modification.^{28,29}

Synthesis of Bare Core NaErF₄ Nanoparticles. In a typical experiment, 1 mmol ErCl₃ was added in a three-neck flask with 6 mL OA and 15 mL ODE. The mixture was stirred at 160 °C for 30 min under an argon atmosphere until a clear light-pink solution was obtained. Then it was cooled down to room temperature. After being added with 5 mL methanol solution containing 2.5 mmol NaOH and 4 mmol NH₄F, the clear solution turned into opacity and was heated to 70 °C for 20 min to remove methanol molecules. With argon gas protection, the solution was rapidly heated to 300 °C and maintained for another 90 min with stirring. The resulting nanoparticles were first washed with acetone and then washed with ethanol twice. Then they were dispersed in 4 mL cyclohexane.

NaYF₄ Precursor. Typically, 2 mmol CF₃COONa and 2 mmol (CF₃COO)₃Y were added into a 100 mL flask with 6 mL OA, 10 mL ODE and 6 mL oleylamine. The mixture was robustly stirred at 160 °C for 30 min to dissolve the reagents. Then the solution was directly heated to 290 °C for 1 h and cooled down to room temperature. The obtained precursor was precipitated by adding excess ethanol. Then after centrifugation, the products were finally redispersed in 4 mL ODE.

NaYb(x)F₄:Tm (0.5 mol %) Precursor. A set of NaYb(x)F₄:0.5% Tm precursor was prepared with increasing concentrations of Yb³⁺ sensitizers (20%, 40%, 60%, 80% and 99.5%). Briefly, Tm₂O₃ (1 mmol) was dissolved in 50% aqueous trifluoroacetic acid (20 mL), refluxed overnight at 95 °C, and dried overnight at 70 °C remaining ~2 mmol Thulium trifluoroacetate as white powder. Similarly, the Ytterbium trifluoroacetate was obtained. The Tm³⁺ concentrations were fixed at 0.5% to ensure a uniform Tm³⁺ content in these samples. Taking NaYbF₄:0.5%Tm precursor as an example, 1.99 mmol (CF₃COO)₃Yb, 0.01 mmol (CF₃COO)₃Tm, 2 mmol CF₃COONa were added into a 100 mL flask with 6 mL OA, 10 mL ODE and 6 mL

oleylamine. The following preparation was conducted in a similar procedure.

General Procedure for the Synthesis of Core–Shell–Shell Nanoparticles (NaYF₄@NaYb(x)Y(99.5% – x)F₄:0.5%Tm@NaYF₄). The synthesis of NaYF₄ core was prepared as the mentioned procedure of NaErF₄. The as-obtained NaYF₄ nanoparticles are dissolved in 11 mL cyclohexane solution for further use. Briefly, 2 mL cyclohexane solution containing 0.5 mmol NaYF₄ bare core nanoparticles were mixed in the 100 mL three-neck flask with 6 mL OA, 15 mL ODE. Protected by argon gas, the solution was rapidly heated to 300 °C. When the solution temperature reached 300 °C, 1 mmol NaYb(x)Y(99.5% – x)F₄:0.5%Tm precursor and 2 mmol NaYF₄ precursor were injected into the solution in sequence, each with a reaction time of 30 min to form corresponding epitaxial shells. After the entire reaction, the mixture was cooled down and the resultant products were collected by centrifugation with acetone once and ethanol twice.

Synthesis of Multishelled Nanoparticles (NaErF₄@NaYF₄@NaYbF₄:0.5%Tm@NaYF₄). The procedure is similar to core–shell–shell nanoparticles and just take the core–shelled NaErF₄@NaYF₄ as bare core. The PUCNPs with two-way of excitation were optimized by varying the doping content to increase shell thickness. According to the results above, NaErF₄@NaYF₄@NaYbF₄:0.5%Tm@NaYF₄ with various shell thicknesses were synthesized.

Synthesis of NaErF₄@NaYF₄@NaYF₄:Nd Nanoparticles. The procedure is similar to the above protocol with different thickness of NaYF₄ layer.

Preparation of PUCNPs@TiO₂ Nanoplatform for PDT. The PUCNPs@TiO₂ nanoplatform was prepared according to the reported method.³⁰ First, the ligand-free of PUCNPs was obtained by removing the surface ligand (oleic acid, OA) on the nanoparticles. Typically, 4 mL 0.1 M HCl solution was added to the 4 mL of PUCNPs-OA cyclohexane solution. And the mixture was stirred vigorously until the PUCNPs were transferred to the water phase, monitored by the 980 nm laser.

The PUCNPs were separated from the below solution and centrifuged at 12 000 rpm for 15 min. After that, the supernatant was discarded and the ligand-free nanoparticles were purified by washing with diwater for three times and finally redispersed for further use. The concentration of PUCNPs was determined by weighing out the dried nanoparticles in solution. Next, 500 mg PVP was dissolved in 4 mL of diwater containing 16 mg of ligand-free PUCNPs. After stirring at RT overnight, 20 mL of absolute ethanol was added to the above solution, then 4 mL of TiF₄ solution (3 mg/mL) was added dropwise to the solution. Finally, the solution was transferred to the 50 mL of autoclave and kept at 180 °C for 8 h. After the autoclave cooled to RT, the as-prepared PUCNPs@TiO₂ was collected by centrifugation and washed with ethanol and diwater several times, respectively, and then dissolved in water for further use.

Detection of Reactive Oxygen Species (ROS). ROS was detected by FCLA according to a previously published method.³¹ First of all, to confirm the photoswitch manner of ROS generation, the time-dependent ROS production at the same concentration of PUCNPs@TiO₂ was studied. Briefly, 1 mL of the reaction mixture contained PUCNPs@TiO₂ (400 μg/mL), 0.06 μg/mL of FCLA (prepared just before use) and 0.01 M PBS (pH 7.4) in a standard quartz cuvette (1 × 1 × 4 cm). Then the mixture was irradiated by 800 and 980 nm lasers light (for 0, 5, 10, 15 min) at the same photodensity of 0.5 W/cm². After separated from the PUCNPs@TiO₂ nanoparticles by centrifugation, the supernatant was immediately measured by fluorescence spectrometer, respectively. Then, the concentration-dependent ROS production was also studied. Similar experimental methods were performed. The concentration of ROS produced by PUCNPs@TiO₂ (a serial of concentrations) under 980 or 800 nm excitation at 0.5 W/cm². To guarantee that there is enough dissolved oxygen, we only irradiated for 5 min with stirring.

The generation of ROS was also confirmed by the intracellular experiment using DCFH-DA probe. Typically, A549 cells were seeded on the glass bottom of cell-culture plates at a density of 1.5 × 10⁴ cells/well. After that, the cells were incubated with PUCNPs@TiO₂

(200 μg/mL) at 37 °C for 12 h and then treated with DCFH-DA (10 μM) at 37 °C for 20 min. The culture medium was discharged and the cells were rinsed with medium. Finally, the cells were treated with 800 and 980 nm laser at 0.5 W/cm² power density for 10 min, respectively. The fluorescence intensity of the cells was evaluated by confocal laser scanning microscopy (CLSM) (Ex = 488 nm and Em = 500–540 nm).

800 nm for Real-Time Cellular Imaging and 980 nm for PDT with Photoswitchable Smart PUCNPs Nanoplatform *In Vitro*.

On the basis of the smart multifunctional two-way of NIR photoswitch PUCNPs. As a proof of concept, we performed the real-time image-guided PDT in A549 cells. Briefly, the cellular uptake profiles and irradiation wavelength dependent cytotoxicity were evaluated.

For cellular imaging, A549 cells were seeded on the cell-culture plates (1.5 × 10⁴ cells/well) for 24 h. Then the medium was replaced by the fresh medium containing PUCNPs@TiO₂ nanoplatform, followed by another 12 h incubation. Afterward, the cells were rinsed with PBS, fixed with immunol staining fix solution and stained with DAPI for 5 min. Then it was examined by a modified CLSM with an upconversion system (Nikon microscope equipped with 980 and 800 nm lasers) upon different excitation wavelengths.

For PDT study, A549 cells were seeded in 96-well plates at a density of 1 × 10⁴ cells per well. After confluent growth for 24 h, the culture medium was discharged and the cells were incubated with fresh medium containing various concentration of PUCNPs@TiO₂. A standard MTT method was explored to examine the cytotoxicity of as-prepared PUCNPs@TiO₂ after another 24 h incubation. On the basis of dark cytotoxicity results, the *in vitro* PDT was carried out. The same concentration of PUCNPs@TiO₂ and the same irradiation power densities (1 W/cm²) under 800 and 980 nm light were exposed to the predetermined concentration of cell wells for 15 min, respectively. Similarly, the cell viability was evaluated by MTT assay.

Photoswitching PDT and Imaging *In Vivo*. All the animal studies were approved in conformity with the animal management protocols. The tumor-bearing mice were successfully obtained by the subcutaneous injection of mouse Lewis lung carcinoma (LLC) cells into C57BL/6 mice. When the tumors were grown to a size of around 50 mm³, the tumor-bearing mice were randomly assigned into six different groups: (i) untreated control, (ii) control (980 nm NIR-light alone), (iii) control (800 nm NIR-light alone) (iv) PUCNPs@TiO₂ alone, (v) PUCNPs@TiO₂ with 800 nm laser light, and (vi) PUCNPs@TiO₂ with 980 nm PDT, and each group contained of 5 mice. Except for the control groups, all the other groups were intravenously injected with 100 μL of PUCNPs@TiO₂ (10 mg/mL) but with different treatment strategies. Tumor size was measured after treated for 2 weeks. The calculation of tumor volume was conducted by applying the following formula: Volume = (ab²/2), where *a* and *b* are tumor dimensions in 2 orthogonal directions. All the animals were sacrificed at day 14. Xenografts were dissected free of surrounding tissue and fixed with 4% paraformaldehyde. *In vivo* UCL imaging was performed with an IVIS spectrum, modified with the equipment of an 800 nm CW laser as the excitation source.

ASSOCIATED CONTENT

Supporting Information

The Supporting Information is available free of charge on the ACS Publications website at DOI: 10.1021/acsnano.7b07393.

- (A) XRD patterns of NaErF₄, NaErF₄@NaYF₄, NaErF₄@NaYF₄@NaYbF₄:Tm and NaErF₄@NaYF₄@NaYbF₄:Tm@NaYF₄; (B) Upconversion emission spectra of (a) NaErF₄@NaYF₄ and NaYF₄:20%Yb, 2% Er@20%Yb@20%Nd (800 nm); (b) NaErF₄@NaYF₄ and NaYF₄:20%Yb, 2%Er @NaYF₄ (980 nm); (C) The upconversion emission of PUCNPs with S1 (NaYF₄) layer 3 and 4.5 nm upon 980 nm laser excitation, respectively; (D) TEM images of as-prepared various UCNPs to study the ions diffusion effect; UC emission spectra of various UCNPs for comparison to study diffusion effect; The discussion of Nd³⁺ diffusion effect;

(E) SEM images of NaYF₄@NaYF₄:x%Yb, 0.5%Tm@NaYF₄ (x = 20 to 99.5%); (F) Cell viabilities of A549 cells treated with PUCNPs@TiO₂; (G) Consumption of FCLA resulted by PUCNPs@TiO₂; (H) Laser-induced ROS generation of the PUCNPs@TiO₂ in A549 cells using DCFH-DA probe; (I) H&E staining of various organ tissues (PDF)

AUTHOR INFORMATION

Corresponding Authors

*E-mail: yuleichang@ciomp.ac.cn.

*E-mail: h.zhang@uva.nl.

*E-mail: xgkong14@ciomp.ac.cn.

ORCID

Yulei Chang: 0000-0001-7223-1797

Author Contributions

[†]J. Zuo and L. Tu contributed equally to this work.

Notes

The authors declare no competing financial interest.

ACKNOWLEDGMENTS

This work was financially supported by the National Natural Science Foundation of China (11474278, 11374297, 61575194, 11674316, 11504371 and 11604331), Project of Science and Technology Agency, Jilin Province (20170520112JH, 20170520113JH and 20170519002JH), Joint research program between CAS of China and KNAW of The Netherlands, European Union MSCA-ITN-2015-ETN Action program, ISPIC, under grant no. 675743 and Netherlands Organization for Scientific Research in the framework of the Fund New Chemical Innovation (2015) TA under grant no. 731.015.206, EU COST program no. 1403. Project supported by State Key Laboratory of Luminescence and Applications.

REFERENCES

- (1) Bordat, P.; Brown, R. Elucidation of Optical Switching of Single Guest Molecules in Terrylene/*p*-Terphenyl Mixed Crystals. *Chem. Phys. Lett.* **2000**, *331*, 439–445.
- (2) Ando, R.; Mizuno, H.; Miyawaki, A. Regulated Fast Nucleocytoplasmic Shuttling Observed by Reversible Protein High-lighting. *Science* **2004**, *306*, 1370–1373.
- (3) Bossi, M.; Belov, V.; Polyakova, S.; Hell, S. W. Reversible Red Fluorescent Molecular Switches. *Angew. Chem., Int. Ed.* **2006**, *45*, 7462–7465.
- (4) Irie, M.; Fukaminato, T.; Sasaki, T.; Tamai, N.; Kawai, T. Organic Chemistry: A Digital Fluorescent Molecular Photoswitch. *Nature* **2002**, *420*, 759–760.
- (5) Fukaminato, T. Single-Molecule Fluorescence Photoswitching: Design and Synthesis of Photoswitchable Fluorescent Molecules. *J. Photochem. Photobiol., C* **2011**, *12*, 177–208.
- (6) Shaner, N. C.; Lin, M. Z.; McKeown, M. R.; Steinbach, P. A.; Hazelwood, K. L.; Davidson, M. W.; Tsien, R. Y. Improving the Photostability of Bright Monomeric Orange and Red Fluorescent Proteins. *Nat. Methods* **2008**, *5*, 545–551.
- (7) Ha, T.; Tinnefeld, P. Photophysics of Fluorescent Probes for Single-Molecule Biophysics and Super-Resolution Imaging. *Annu. Rev. Phys. Chem.* **2012**, *63*, 595–617.
- (8) Liu, Y.; Lu, Y.; Yang, X.; Zheng, X.; Wen, S.; Wang, F.; Vidal, X.; Zhao, J.; Liu, D.; Zhou, Z.; Ma, C.; Zhou, J.; Piper, J. A.; Xi, P.; Jin, D. Amplified Stimulated Emission in Upconversion Nanoparticles for Super-Resolution Nanoscopy. *Nature* **2017**, *543*, 229–233.
- (9) Ong, L. C.; Ang, L. Y.; Alonso, S.; Zhang, Y. Bacterial Imaging with Photostable Upconversion Fluorescent Nanoparticles. *Biomaterials* **2014**, *35*, 2987–2998.

- (10) Lai, J.; Zhang, Y.; Pasquale, N.; Lee, K. B. An Upconversion Nanoparticle with Orthogonal Emissions Using Dual NIR Excitations for Controlled Two-Way Photoswitching. *Angew. Chem., Int. Ed.* **2014**, *53*, 14419–14423.

- (11) Li, X.; Guo, Z.; Zhao, T.; Lu, Y.; Zhou, L.; Zhao, D.; Zhang, F. Filtration Shell Mediated Power Density Independent Orthogonal Excitations-Emissions Upconversion Luminescence. *Angew. Chem., Int. Ed.* **2016**, *55*, 2464–2469.

- (12) Wang, L.; Dong, H.; Li, Y. N.; Liu, R.; Wang, Y. F.; Bisoyi, H. K.; Sun, L. D.; Yan, C. H.; Li, Q. Luminescence-Driven Reversible Handedness Inversion of Self-Organized Helical Superstructures Enabled by a Novel Near-Infrared Light Nanotransducer. *Adv. Mater.* **2015**, *27*, 2065–2069.

- (13) Zheng, W.; Huang, P.; Tu, D.; Ma, E.; Zhu, H.; Chen, X. Lanthanide-Doped Upconversion Nano-Bioprobes: Electronic Structures, Optical Properties, and Biodetection. *Chem. Soc. Rev.* **2015**, *44*, 1379–1415.

- (14) Yang, G.; Yang, D.; Yang, P.; Lv, R.; Li, C.; Zhong, C.; He, F.; Gai, S.; Lin, J. A Single 808 nm Near-Infrared Light-Mediated Multiple Imaging and Photodynamic Therapy Based on Titania Coupled Upconversion Nanoparticles. *Chem. Mater.* **2015**, *27*, 7957–7968.

- (15) Lv, R. C.; Yang, P. P.; He, F.; Gai, S. L.; Li, C. X.; Dai, Y. L.; Yang, G. X.; Lin, J. A Yolk-Like Multifunctional Platform for Multimodal Imaging and Synergistic Therapy Triggered by a Single Near-Infrared Light. *ACS Nano* **2015**, *9*, 1630–1647.

- (16) Wang, Y. F.; Liu, G. Y.; Sun, L. D.; Xiao, J. W.; Zhou, J. C.; Yan, C. H. Nd³⁺-Sensitized Upconversion Nanophosphors: Efficient *In Vivo* Bioimaging Probes with Minimized Heating Effect. *ACS Nano* **2013**, *7*, 7200–7206.

- (17) Wang, D.; Xue, B.; Kong, X.; Tu, L.; Liu, X.; Zhang, Y.; Chang, Y.; Luo, Y.; Zhao, H.; Zhang, H. 808 nm Driven Nd³⁺-Sensitized Upconversion Nanostructures for Photodynamic Therapy and Simultaneous Fluorescence Imaging. *Nanoscale* **2015**, *7*, 190–197.

- (18) Xie, X.; Gao, N.; Deng, R.; Sun, Q.; Xu, Q. H.; Liu, X. Mechanistic Investigation of Photon Upconversion in Nd³⁺-Sensitized Core-Shell Nanoparticles. *J. Am. Chem. Soc.* **2013**, *135*, 12608–12611.

- (19) Boyer, J. C.; Carling, C. J.; Gates, B. D.; Branda, N. R. Two-Way Photoswitching Using One Type of Near-Infrared Light, Upconverting Nanoparticles, and Changing Only the Light Intensity. *J. Am. Chem. Soc.* **2010**, *132*, 15766–15772.

- (20) Li, W.; Chen, Z.; Zhou, L.; Li, Z.; Ren, J.; Qu, X. Noninvasive and Reversible Cell Adhesion and Detachment via Single-Wavelength Near-Infrared Laser Mediated Photoisomerization. *J. Am. Chem. Soc.* **2015**, *137*, 8199–8205.

- (21) Wang, P.; Li, X.; Yao, C.; Wang, W.; Zhao, M.; El-Toni, A. M.; Zhang, F. Orthogonal Near-Infrared Upconversion Co-Regulated Site-Specific O₂ Delivery and Photodynamic Therapy For Hypoxia Tumor by Using Red Blood Cell Microcarriers. *Biomaterials* **2017**, *125*, 90–100.

- (22) Tu, L. P.; Liu, X. M.; Wu, F.; Zhang, H. Excitation Energy Migration Dynamics in Upconversion Nanomaterials. *Chem. Soc. Rev.* **2015**, *44*, 1331–1345.

- (23) Johnson, N. J.; He, S.; Diao, S.; Chan, E. M.; Dai, H.; Almutairi, A. Direct Evidence for Coupled Surface and Concentration Quenching Dynamics in Lanthanide-Doped Nanocrystals. *J. Am. Chem. Soc.* **2017**, *139*, 3275–3282.

- (24) Chen, Q.; Xie, X.; Huang, B.; Liang, L.; Han, S.; Yi, Z.; Wang, Y.; Li, Y.; Fan, D.; Huang, L.; Liu, X. Confining Excitation Energy in Er³⁺-Sensitized Upconversion Nanocrystals through Tm³⁺-Mediated Transient Energy Trapping. *Angew. Chem., Int. Ed.* **2017**, *56*, 7605–7609.

- (25) Zuo, J.; Li, Q.; Xue, B.; Li, C.; Chang, Y.; Zhang, Y.; Liu, X.; Tu, L.; Zhang, H.; Kong, X. Employing Shells to Eliminate Concentration Quenching in Photonic Upconversion Nanostructure. *Nanoscale* **2017**, *9*, 7941–7946.

- (26) Chen, X.; Jin, L.; Kong, W.; Sun, T.; Zhang, W.; Liu, X.; Fan, J.; Yu, S. F.; Wang, F. Confining Energy Migration in Upconversion Nanoparticles Towards Deep Ultraviolet Lasing. *Nat. Commun.* **2016**, *7*, 10304.

(27) Liu, Y. Y.; Liu, Y.; Bu, W. B.; Cheng, C.; Zuo, C. J.; Xiao, Q. F.; Sun, Y.; Ni, D. L.; Zhang, C.; Liu, J. A.; Shi, J. L. Hypoxia Induced by Upconversion-Based Photodynamic Therapy: Towards Highly Effective Synergistic Bioreductive Therapy in Tumors. *Angew. Chem., Int. Ed.* **2015**, *54*, 8105–8109.

(28) Johnson, N. J.; Korinek, A.; Dong, C.; van Veggel, F. C. Self-Focusing by Ostwald Ripening: A Strategy for Layer-by-Layer Epitaxial Growth on Upconverting Nanocrystals. *J. Am. Chem. Soc.* **2012**, *134*, 11068–11071.

(29) Qian, H. S.; Zhang, Y. Synthesis of Hexagonal-Phase Core-Shell NaYF₄ Nanocrystals with Tunable Upconversion Fluorescence. *Langmuir* **2008**, *24*, 12123–12125.

(30) Hou, Z. Y.; Zhang, Y. X.; Deng, K. R.; Chen, Y. Y.; Li, X. J.; Deng, X. R.; Cheng, Z. Y.; Lian, H. Z.; Li, C. X.; Lin, J. UV-Emitting Upconversion-Based TiO₂ Photosensitizing Nanoplatform: Near-Infrared Light Mediated *in Vivo* Photodynamic Therapy via Mitochondria-Involved Apoptosis Pathway. *ACS Nano* **2015**, *9*, 2584–2599.

(31) Zhou, A. G.; Wei, Y. C.; Wu, B. Y.; Chen, Q.; Xing, D. Pyropheophorbide A and c(RGDyK) Comodified Chitosan-Wrapped Upconversion Nanoparticle for Targeted Near-Infrared Photodynamic Therapy. *Mol. Pharmaceutics* **2012**, *9*, 1580–1589.